

Dynamical generation of low-energy couplings from quark-meson fluctuations

Florian Divotgey,^{1,*} Jürgen Eser,^{1,†} and Mario Mitter^{2,‡}

¹*Institut für Theoretische Physik, Johann Wolfgang Goethe-Universität,
Max-von-Laue-Straße 1, D-60438 Frankfurt am Main, Germany*

²*Department of Physics, Brookhaven National Laboratory, Upton, NY 11973, USA*
(Dated: January 10, 2019)

We extend our recent computation of the low-energy limit of the linear $O(4)$ Quark-Meson Model. The present analysis focuses on the transformation of the resulting effective action into a nonlinearly realized effective pion action, whose higher-derivative interaction terms are parametrized by so-called low-energy couplings. Their counterparts in the linear model are determined from the Functional Renormalization Group flow of the momentum-dependent four-pion vertex, which is calculated in a fully $O(4)$ -symmetric approximation by including also momentum-dependent $\sigma\pi$ interactions as well as σ self-interactions. Consequently, these higher-derivative couplings are dynamically generated solely from quark and meson fluctuations, initialized at a hadronic scale. Despite our restriction to low-energy degrees of freedom, we find that the qualitative features of the fluctuation dynamics allow us to comment on the range of validity and on appropriate renormalization scales for purely pionic effective models.

PACS numbers: 11.10.Hi, 12.39.Fe

I. INTRODUCTION

A time-honored possibility to study the low-energy regime of the theory of strong interactions, Quantum Chromodynamics (QCD), is given by Effective Field Theories (EFTs). In this approach, one investigates QCD-inspired effective models that describe the interactions of the relevant low-energy degrees of freedom, namely, those of hadrons. In order to capture the low-energy dynamics of the strong interaction properly, the construction of these models is mainly based on the internal and space-time symmetries of QCD and their possible breaking.

In the context of low-energy models for QCD, the most central symmetry is given by the chiral $SU(N_f)_L \times SU(N_f)_R$ symmetry accidentally arising from the quark sector of the QCD Lagrangian. Here, N_f refers to the number of dynamical quark flavors, which will be set to two, $N_f = 2$, throughout the rest of this work.

The importance of chiral symmetry is twofold: On the one hand, the hadronic currents arise as multiplets with respect to the chiral group. Therefore, group theory allows for a systematic construction of chirally invariant Lagrangians. On the other hand, the explicit and spontaneous breaking of chiral symmetry is of immediate physical relevance. In particular, one observes so-called pseudo Nambu-Goldstone bosons (pNGBs) in the associated particle spectrum. Since these particles are very light, they dominate the low-energy dynamics of the theory and, consequently, are of crucial importance for a proper low-energy description. In the case of two-flavor QCD, these pNGBs are associated with the pion fields.

In the framework of QCD, the most important example of an EFT is given by Chiral Perturbation Theory (ChPT) [1, 2]. Conceptually, this approach corresponds to a simultaneous expansion of the QCD generating functional in powers of pion momenta and quark masses. The associated effective Lagrangian contains an infinite tower of pion self-interactions coupled by so-called low-energy constants (LECs). These coupling constants encode essential information about the low-energy regime of QCD. At lowest order in the chiral expansion, the ChPT Lagrangian is equivalent to the Nonlinear Sigma Model (NLSM) [3].

Apart from ChPT, it is also possible to construct effective low-energy models from a linear realization of chiral symmetry. The resulting family of models is usually referred to as Linear Sigma Models (LSMs). In contrast to the nonlinear models, the pNGB fields and their chiral partners are here treated on the same footing. The simplest and most prominent example of such a model is given by the $O(4)$ LSM, which describes the interaction of the σ meson and the three pions.

In a recent work [4], we studied the low-energy limit of the $O(4)$ LSM coupled to quarks, the so-called Quark-Meson Model (QMM), within the Functional Renormalization Group (FRG) approach. Besides the Yukawa coupling of the scalar and pseudoscalar mesons to the quark fields, the $O(4)$ LSM has been extended by complete sets of derivative couplings of order $\mathcal{O}(\partial^2)$ and $\mathcal{O}(\partial^4)$ for the pion fields. This corresponds to an approximation well beyond the usual local potential approximation (LPA) and LPA' truncations, where these derivative couplings are solely generated from meson and quark fluctuations.

After its calculation from the FRG flow, the effective action of the QMM has been reduced to an effective pion action by integrating out the σ field, similarly to Refs. [5, 6]. In this action, the higher-derivative terms are parametrized by the low-energy couplings of the $O(4)$

* fdivotgey@th.physik.uni-frankfurt.de

† eser@th.physik.uni-frankfurt.de

‡ mitter@bnl.gov

QMM.

In the present work, we improve and extend the previous analysis of these low-energy couplings in several crucial ways:

- (i) We transform the effective action of the QMM into a nonlinearly realized pion action by explicitly restricting the dynamics of the system onto the vacuum manifold $SO(4)/SO(3)$. This manifold is associated to the spontaneous breakdown of the $O(4)$ symmetry. After choosing a specific set of coordinates on $SO(4)/SO(3)$, we will deduce relations between the higher-derivative couplings in the linearly realized QMM and the nonlinear model featuring only pion dynamics. This nonlinear model is then referred to as the low-energy limit of the QMM within this work.
- (ii) In order to determine the range of validity of the low-energy effective theory, we investigate the relative importance of mesonic and fermionic loop contributions to the renormalization group (RG)-scale dependence of the low-energy couplings in the nonlinear model.
- (iii) We introduce the higher-derivative couplings in the linear model in a completely $O(4)$ -invariant manner, i.e., taking also momentum dependences of the interaction of the pion fields with the σ meson into account, and also include a scale dependence of the Yukawa interaction.

The paper is organized as follows: In Secs. II and III, we introduce the basic models, methods, and concepts that are used in this work. To this end, Secs. II A and II B briefly review the $O(4)$ LSM, the NLSM, as well as the nonlinear formalism. Afterwards, Sec. III A focuses on the higher-derivative interactions in terms of the FRG truncation. In Sec. III B, we transform the linearly realized effective action of the QMM into its nonlinear counterpart. Finally, Sec. IV presents the numerical results of the FRG flow within the linear QMM, cf. Sec. IV A, and the computed low-energy couplings of the associated nonlinear model, cf. Sec. IV B. The conclusions of this work as well as an outlook for further investigations is given in Sec. V.

II. MODELS

In this section, we briefly summarize the most important features of the linear QMM and the nonlinear model with pionic degrees of freedom.

A. The linear Quark-Meson Model

As already mentioned in the introduction, the simplest model based on a linear realization of chiral symmetry is

given by the $O(4)$ LSM. The basic object of this model is the four-dimensional Euclidean field-space vector

$$\varphi = \begin{pmatrix} \vec{\pi} \\ \sigma \end{pmatrix}. \quad (1)$$

This vector constitutes the fundamental representation of $O(4)$ and, hence, transforms as

$$\varphi \xrightarrow{O(4)} O\varphi, \quad O \in O(4). \quad (2)$$

The Lagrangian of the $O(4)$ LSM is then constructed as

$$\mathcal{L}_{\text{LSM}} = \frac{1}{2} (\partial_\mu \varphi) \cdot \partial^\mu \varphi - \frac{m_0^2}{2} \varphi \cdot \varphi - \frac{\lambda}{4} (\varphi \cdot \varphi)^2. \quad (3)$$

The QMM is obtained from the above Lagrangian by including quarks in a chirally invariant way,

$$\begin{aligned} \mathcal{L}_{\text{QMM}} = & \frac{1}{2} (\partial_\mu \varphi) \cdot \partial^\mu \varphi - \frac{m_0^2}{2} \varphi \cdot \varphi - \frac{\lambda}{4} (\varphi \cdot \varphi)^2 + h_{\text{ESB}} \sigma \\ & + \bar{\psi} (i\gamma^\mu \partial_\mu - y\Phi_5) \psi, \end{aligned} \quad (4)$$

with

$$\Phi_5 = \sigma t_0 + i\gamma_5 \vec{\pi} \cdot \vec{t}, \quad (5)$$

where $t_0 = \mathbb{1}_2/2$ and $\vec{t} = \vec{\tau}/2$. Here, $\vec{\tau}$ denotes the usual vector of the Pauli matrices. The normalization of the generators is chosen such that $\text{tr}(t_a t_b) = \delta_{ab}/2$, $a, b = 0, \dots, 3$. The additional term $\sim h_{\text{ESB}} \sigma$ in the above Lagrangian describes the explicit breaking of chiral symmetry (ESB) by tilting the mesonic potential into the direction of the σ field.

In addition to the ESB, also the spontaneous breaking of chiral symmetry has to be modelled. The latter is signaled by a nonvanishing order parameter identified with the vacuum expectation value σ_0 of the σ field. This order parameter is typically introduced by shifting the σ field according to

$$\sigma \rightarrow \sigma_0 + \sigma. \quad (6)$$

B. The nonlinear model

In contrast to the LSM, described by Eq. (3), the field space of the associated nonlinear model is not given by the four-dimensional Euclidean space, but by a three-dimensional submanifold [7]. This field space arises as a consequence of the pattern of spontaneous symmetry breaking. It is defined by the degenerate vacua and is usually denoted as the vacuum manifold. Since the coordinates of this space are in one-to-one correspondence with the pNGBs, the basic degrees of freedom of the NLSM are given by the three pion fields.

For the following discussion, we only consider the $SO(4)$ subgroup of $O(4)$, such that the vacuum manifold of the LSM is given by the space of (left) cosets $SO(4)/SO(3)$, cf. Refs. [8–10]. Using a representative of

this coset space, in the following denoted as $\Sigma(\zeta)$, it is possible to construct the so-called Maurer-Cartan form $\alpha_\mu(\zeta)$ as

$$\alpha_\mu(\zeta) = \Sigma^{-1}(\zeta) \partial_\mu \Sigma(\zeta). \quad (7)$$

It should be emphasized that the coordinates of the coset space, ζ^α , $\alpha = 1, 2, 3$, are usually not exactly identical to the pion fields, but directly related to them. The Maurer-Cartan form is defined in the Lie algebra $\mathfrak{so}(4)$ and can therefore be expanded as

$$\alpha_\mu(\zeta) = ie_\mu^a(\zeta) x_a + i\omega_\mu^i(\zeta) s_i, \quad (8)$$

with coefficients

$$e_\mu^a(\zeta) = e_\alpha^a(\zeta) \partial_\mu \zeta^\alpha, \quad \omega_\mu^i(\zeta) = \omega_\alpha^i(\zeta) \partial_\mu \zeta^\alpha, \quad (9)$$

where x_a , $a = 1, 2, 3$, denotes the coset generators and s_i , $i = 1, 2, 3$, those of the unbroken $SO(3)$ subgroup. The coefficients $e_\alpha^a(\zeta)$ define a frame on $SO(4)/SO(3)$ and the related metric reads

$$g_{\alpha\beta}(\zeta) = \delta_{ab} e_\alpha^a(\zeta) e_\beta^b(\zeta), \quad (10)$$

where $\alpha, \beta = 1, 2, 3$ represent curved coset indices.

The simplest Lagrangian that can be constructed from the above objects is given by

$$\mathcal{L}_{\text{NLSM}} = \frac{1}{2} F_{ab} e_\mu^a(\zeta) e^{b,\mu}(\zeta), \quad (11)$$

where the real-valued matrix F is needed for dimensional reasons. This Lagrangian is usually called the $SO(4)$ NLSM and contains the pion self-interaction terms to arbitrary order in the fields with at most two spacetime derivatives.

In Appendix A, we review the general transformation properties of the coset representative and the Maurer-Cartan form. In addition, we present the transformation behavior of the nonlinear pion fields for an explicit choice of coordinates.

III. METHODS

In this section, we discuss the calculation of the linearly realized effective action of the QMM and its relation to the nonlinear model featuring only pionic degrees of freedom.

A necessary prerequisite for the determination of the low-energy couplings of the nonlinear model from the effective action in terms of linearly realized pion fields is the integration of all nonpionic QCD fluctuations, and, in particular, the quark loops. Moreover, such a determination of the low-energy couplings is only meaningful at scales, where fluctuations of nonpionic fields have already decoupled from the dynamics.

Before going on, we want to point out that the quark fluctuations of the QMM simulate full QCD dynamics.

In contrast to the purely mesonic linear model, including these quark fluctuations entails the qualitatively correct decoupling of the mesonic degrees of freedom above the scale of chiral symmetry breaking. Quantitatively, pure quark fluctuations are not capable of fully capturing QCD dynamics and, e.g., this decoupling happens too slowly [11–13]. An investigation of the effect of full QCD dynamics on the determination of the low-energy couplings is deferred to future work.

A. Effective action from the Functional Renormalization Group

The FRG is a nonperturbative continuum method that formulates the integration of quantum fluctuations in terms of the RG-scale (k) dependence of the effective average action Γ_k , which smoothly interpolates between the renormalized classical action S at the ultraviolet (UV) cutoff scale Λ , $\Gamma_{k \rightarrow \Lambda} = S$, and the quantum effective action Γ in the infrared (IR), $\Gamma_{k \rightarrow 0} = \Gamma$. The action Γ is the generating functional for all one-particle irreducible vertex functions.

The scale evolution of Γ_k from the UV to the IR is described by the Wetterich equation [14],

$$\begin{aligned} \partial_k \Gamma_k &= \frac{1}{2} \text{tr} \left[\partial_k R_k \left(\Gamma_k^{(2)} + R_k \right)^{-1} \right] \\ &= \frac{1}{2} \text{tr} \left(\text{circle with cross} \right), \end{aligned} \quad (12)$$

where the second line introduces the common diagrammatical notation

$$\left(\Gamma_k^{(2)} + R_k \right)^{-1} = \text{horizontal line}, \quad \partial_k R_k = \text{circle with cross}. \quad (13)$$

The above flow equation contains the regulator function R_k , which gives an additional mass contribution for low-energy modes. This means that it effectively acts as an IR cutoff separating those soft modes from the integration process. By successively lowering the scale k , the effective average action Γ_k includes increasingly more fluctuations and, in the limit $k \rightarrow 0$, all quantum fluctuations are integrated out.

In order to compute Γ_k , one has to truncate the system of vertex functions, since the right-hand side of Eq. (12) involves the two-point function $\Gamma_k^{(2)}$, which, itself, couples through the flow to higher n -point functions. A typical truncation scheme for these vertex functions is given by a derivative expansion, which we will focus on in the following; cf. also the introductory Refs. [15–25].

Along the lines of our previous study [4], we choose the following (Euclidean) truncation for the linearly realized $O(4)$ QMM based on Eq. (4) in Sec. II A and introduce the k -dependent higher-derivative couplings $C_{2,k}$

and $Z_{2,k}$, as well as $C_{i,k}$, $i = 3, \dots, 8$:

$$\begin{aligned} \Gamma_k = \int_x \left\{ \frac{Z_k}{2} (\partial_\mu \varphi) \cdot \partial_\mu \varphi + U_k - h_{\text{ESB}} \sigma \right. \\ + C_{2,k} (\varphi \cdot \partial_\mu \varphi)^2 + Z_{2,k} \varphi^2 (\partial_\mu \varphi) \cdot \partial_\mu \varphi \\ - C_{3,k} [(\partial_\mu \varphi) \cdot \partial_\mu \varphi]^2 - C_{4,k} [(\partial_\mu \varphi) \cdot \partial_\nu \varphi]^2 \\ - C_{5,k} \varphi \cdot (\partial_\mu \partial_\mu \varphi) (\partial_\nu \varphi) \cdot \partial_\nu \varphi \\ - C_{6,k} \varphi^2 (\partial_\mu \partial_\nu \varphi) \cdot \partial_\mu \partial_\nu \varphi \\ - C_{7,k} (\varphi \cdot \partial_\mu \partial_\mu \varphi)^2 - C_{8,k} \varphi^2 (\partial_\mu \partial_\mu \varphi)^2 \\ \left. + \bar{\psi} \left(Z_k^\psi \gamma_\mu \partial_\mu + y_k \Phi_5 \right) \psi \right\}. \end{aligned} \quad (14)$$

This truncation constitutes a derivative expansion up to order $\mathcal{O}(\partial^4)$. It is well beyond the LPA and its minimal extension known as the LPA'. The first would only consider a scale-dependent effective potential U_k , which is a function of the $O(4)$ invariant ρ ,

$$\rho \equiv \varphi \cdot \varphi = \vec{\pi}^2 + \sigma^2, \quad (15)$$

while the latter would also take into account the scaling of the field variables by means of the flow of the wave-function renormalization factors for bosons and fermions, Z_k and Z_k^ψ . In both of these two approximations, the higher-derivative couplings would be absent, i.e., they are set to zero. In the light of Ref. [4], the momentum-independent coupling $C_{1,k}(\varphi \cdot \varphi)^2$ is omitted in the above equation. It is to be identified with the quartic interaction term of the effective potential.

The parameter $h_{\text{ESB}} \neq 0$ explicitly breaks the $O(4)$ symmetry, as mentioned in the last section, and remains k independent. For the scale-dependent factors Z_k , Z_k^ψ , and the Yukawa interaction y_k we suppress a general field dependence. The couplings $\{C_{2,k}, Z_{2,k}\}$ as well as $\{C_{i,k}\}$, $i = 3, \dots, 8$, beyond the LPA' form a complete set of terms of order $\mathcal{O}(\varphi^4, \partial^2)$ and $\mathcal{O}(\varphi^4, \partial^4)$, respectively. As an extension of Ref. [4] [cf. Eq. (20) therein], the low-energy couplings in Eq. (14) now include momentum-dependent $\sigma\pi$ and σ self-interactions.

On the level of the two-point functions $\Gamma_k^{(2)}$, we define different effective wave-function renormalization factors for the σ and π fields,

$$Z_k^\sigma = Z_k + 2\sigma^2 (Z_{2,k} + C_{2,k}) - 2\sigma^2 p^2 (C_{6,k} + C_{7,k} + C_{8,k}), \quad (16)$$

$$Z_k^\pi = Z_k + 2\sigma^2 Z_{2,k} - 2\sigma^2 p^2 (C_{6,k} + C_{8,k}), \quad (17)$$

where p is the external momentum from the functional derivatives with respect to the fields. The corrections to Z_k in these definitions obviously arise from the presence of the higher-derivative couplings. It should be noted that the distinction between Z_k^σ and Z_k^π is not in contradiction to the $O(4)$ symmetry of the model. As soon as the σ field acquires a nonvanishing expectation value, $\sigma \neq 0$, the wave-function renormalizations will naturally split.

For later reference, we define the following renormalized quantities based on the wave-function renormalization factors Z_k^π and Z_k^ψ :

$$\begin{aligned} \tilde{\sigma} &= \sqrt{Z_k^\pi} \sigma, & \tilde{\vec{\pi}} &= \sqrt{Z_k^\pi} \vec{\pi}, \\ \tilde{\psi} &= \sqrt{Z_k^\psi} \psi, & \tilde{\bar{\psi}} &= \sqrt{Z_k^\psi} \bar{\psi}, \\ \tilde{h}_{\text{ESB}} &= \frac{h_{\text{ESB}}}{\sqrt{Z_k^\pi}}, & \tilde{y}_k &= \frac{y_k}{Z_k^\psi \sqrt{Z_k^\pi}}, \\ \tilde{C}_{i,k} &= \frac{C_{i,k}}{(Z_k^\pi)^2}, & i &= 1, \dots, 8, & \tilde{Z}_{2,k} &= \frac{Z_{2,k}}{(Z_k^\pi)^2}, \end{aligned} \quad (18)$$

where we will, for simplicity, evaluate the above wave-function renormalization factors at vanishing external momentum, $p = 0$; cf. the discussion in Appendix B. By choosing Z_k^π for both bosonic fields in the definitions (18) one directly obtains the correct renormalization factors in the nonlinear model, as presented in the next section.

The flow equations for all scale-dependent quantities in truncation (14) are obtained by projecting the functional derivatives of Eq. (12) (the flows of vertex functions) onto the respective coupling. The resulting expressions for these equations and further technical aspects, such as the regulator functions, are shown in Appendix B.

Finally, the integration of the coupled system of differential equations then allows for a computation of the quantities in the linearly realized effective average action (14) in the IR limit, $\Gamma_{k \rightarrow 0} = \Gamma$; see Appendix C for details.

B. Effective pion action

A physically meaningful transition from the effective action to the nonlinear model as effective low-energy theory requires that all fluctuations, except for those of the pions, should have decoupled from the dynamics at the energy-momentum scale, where this transition is to be realized. The low-energy limit of the effective action (14), expressed in terms of the renormalized quantities (18), is then constructed by integrating out all (already decoupled) fields,

$$\Gamma_k [\tilde{\sigma}, \tilde{\vec{\pi}}, \tilde{\psi}, \tilde{\bar{\psi}}] \longrightarrow \Gamma_k [\tilde{\vec{\Pi}}]. \quad (19)$$

The vector $\tilde{\vec{\Pi}} = (\tilde{\Pi}^1, \tilde{\Pi}^2, \tilde{\Pi}^3)$ represents the renormalized nonlinear pNGB fields, which will be defined below, and the symbol Γ_k is kept for the resulting action.

The quark fields are immediately dropped from the effective action, similarly to the investigations in Refs. [4, 6], since this integration process is restricted to (at most) tree-level diagrams. As a consequence, Γ_k reduces to the effective action of the usual LSM, modified by the higher-derivative couplings.

As already mentioned in Sec. II B, the $SO(4)$ NLSM is defined on the coset space $SO(4)/SO(3)$, which is diffeomorphic to the three-sphere S^3 . The explicit diffeomor-

phism is given by

$$\tilde{\varphi} \equiv \sqrt{Z_k^\pi} \varphi = \Sigma(\tilde{\zeta}) \tilde{\phi}, \quad (20)$$

with $\tilde{\phi} = (\vec{0}, \tilde{\theta})$, where $\tilde{\theta} = \sqrt{\tilde{\zeta}^2}$ defines the radius of the three-sphere. For the time being, we keep the field $\tilde{\theta}$ and allow fluctuations in radial direction.

The coordinates $\tilde{\zeta}^a$ parametrizing the coset representative $\Sigma(\tilde{\zeta})$ are chosen as stereographic projections,

$$\tilde{\zeta}^a = \frac{\tilde{\pi}^a}{\tilde{\theta} + \tilde{\sigma}}, \quad a = 1, 2, 3, \quad (21)$$

where $\tilde{\pi}^a$ and $\tilde{\sigma}$ are the renormalized Euclidean coordinates of the linear QMM, cf. Sec. III A. An explicit parametrization of the coset representative then reads

$$\Sigma(\tilde{\zeta}) = \begin{pmatrix} \delta^a_b - \frac{2\tilde{\zeta}^a \tilde{\zeta}_b}{1+\tilde{\zeta}^2} & \frac{2\tilde{\zeta}^a}{1+\tilde{\zeta}^2} \\ -\frac{2\tilde{\zeta}_b}{1+\tilde{\zeta}^2} & \frac{1-\tilde{\zeta}^2}{1+\tilde{\zeta}^2} \end{pmatrix}. \quad (22)$$

The coefficients of the Maurer-Cartan form proportional to the broken generators as well as the metric in Eq. (10) are thus evaluated as

$$e_\mu^a(\tilde{\zeta}) \equiv e_\alpha^a(\tilde{\zeta}) \partial_\mu \tilde{\zeta}^\alpha = \frac{2\delta_\alpha^a}{1+\tilde{\zeta}^2} \partial_\mu \tilde{\zeta}^\alpha, \quad (23)$$

and

$$g_{\alpha\beta} \equiv g_{\alpha\beta}(\tilde{\zeta}) = \frac{4\delta_{\alpha\beta}}{(1+\tilde{\zeta}^2)^2}, \quad (24)$$

respectively.

The transition of the LSM to its associated NLSM is now realized by inserting Eq. (20) into Eq. (14) and identifying the $\tilde{\theta}$ field with the pion decay constant f_π [PCAC relation; cf. Ref. [4]],

$$\tilde{\theta} = f_\pi. \quad (25)$$

This step fixes the radial fluctuations $\tilde{\theta}$ to a constant radius and eliminates the $\tilde{\theta}$ field from the effective action. The resulting nonlinear model can then be written as

$$\begin{aligned} \Gamma_k = \int_x \left\{ \frac{f_\pi^2}{2} g_{\alpha\beta} (\nabla_\mu \tilde{\zeta}^\alpha) \nabla_\mu \tilde{\zeta}^\beta \right. \\ - (\tilde{C}_{6,k} + \tilde{C}_{8,k}) f_\pi^4 g_{\alpha\beta} (\nabla_\mu \nabla_\mu \tilde{\zeta}^\alpha) (\nabla_\nu \nabla_\nu \tilde{\zeta}^\beta) \\ - (\tilde{C}_{3,k} - \tilde{C}_{5,k} + \tilde{C}_{6,k} + \tilde{C}_{7,k} + \tilde{C}_{8,k}) f_\pi^4 \\ \times g_{\alpha\beta} g_{\gamma\delta} (\nabla_\mu \tilde{\zeta}^\alpha) (\nabla_\mu \tilde{\zeta}^\beta) (\nabla_\nu \tilde{\zeta}^\gamma) \nabla_\nu \tilde{\zeta}^\delta \\ - \tilde{C}_{4,k} f_\pi^4 g_{\alpha\beta} g_{\gamma\delta} (\nabla_\mu \tilde{\zeta}^\alpha) (\nabla_\nu \tilde{\zeta}^\beta) (\nabla_\mu \tilde{\zeta}^\gamma) \nabla_\nu \tilde{\zeta}^\delta \\ \left. - \tilde{h}_{\text{ESB}} f_\pi \frac{1-\tilde{\zeta}^2}{1+\tilde{\zeta}^2} \right\}, \quad (26) \end{aligned}$$

with $\nabla_\mu \tilde{\zeta}^\alpha \equiv \partial_\mu \tilde{\zeta}^\alpha$. The action of the covariant derivative ∇_μ on a vector $\partial_\nu \tilde{\zeta}^\alpha$ is defined as

$$\nabla_\mu \nabla_\nu \tilde{\zeta}^\alpha \equiv \nabla_\mu \partial_\nu \tilde{\zeta}^\alpha = \partial_\mu \partial_\nu \tilde{\zeta}^\alpha + \Gamma^\alpha_{\beta\gamma} (\partial_\mu \tilde{\zeta}^\beta) \partial_\nu \tilde{\zeta}^\gamma. \quad (27)$$

In stereographic coordinates, the above Christoffel symbols $\Gamma^\alpha_{\beta\gamma}$ read

$$\Gamma^\alpha_{\beta\gamma} = \frac{2}{1+\tilde{\zeta}^2} \left(-\delta^\alpha_\gamma \tilde{\zeta}_\beta - \delta^\alpha_\beta \tilde{\zeta}_\gamma + \delta_{\beta\gamma} \tilde{\zeta}^\alpha \right). \quad (28)$$

The effective action (26) resembles Eq. (11) with $F_{ab} = f_\pi^2 \delta_{ab}$ for these specific coordinates. Furthermore, it features corrections from the ESB term and the higher-derivative couplings. Its general form is consistent with the studies on nonlinear sigma models in Refs. [26, 27].

In order to obtain a canonically normalized kinetic term for the pNGB fields, we introduce a field redefinition according to

$$\tilde{\zeta}^a \rightarrow \frac{\tilde{\Pi}^a}{2f_\pi}, \quad a = 1, 2, 3. \quad (29)$$

Expanding all quantities up to fourth order in the new field variables $\tilde{\Pi}^a$, the above effective action becomes

$$\begin{aligned} \Gamma_k = \int_x \left\{ \frac{1}{2} (\partial_\mu \tilde{\Pi}_a) \partial_\mu \tilde{\Pi}^a + \frac{1}{2} \mathcal{M}_{\Pi,k}^2 \tilde{\Pi}_a \tilde{\Pi}^a \right. \\ - \tilde{C}_{1,k} (\tilde{\Pi}_a \tilde{\Pi}^a)^2 + \tilde{Z}_{2,k} \tilde{\Pi}_a \tilde{\Pi}^a (\partial_\mu \tilde{\Pi}_b) \partial_\mu \tilde{\Pi}^b \\ - \tilde{C}_{3,k} [(\partial_\mu \tilde{\Pi}_a) \partial_\mu \tilde{\Pi}^a]^2 \\ - \tilde{C}_{4,k} [(\partial_\mu \tilde{\Pi}_a) \partial_\nu \tilde{\Pi}^a]^2 \\ - \tilde{C}_{5,k} \tilde{\Pi}_a (\partial_\mu \partial_\mu \tilde{\Pi}^a) (\partial_\nu \tilde{\Pi}_b) \partial_\nu \tilde{\Pi}^b \\ - \tilde{C}_{6,k} \tilde{\Pi}_a \tilde{\Pi}^a (\partial_\mu \partial_\nu \tilde{\Pi}_b) \partial_\mu \partial_\nu \tilde{\Pi}^b \\ \left. - \tilde{C}_{8,k} \tilde{\Pi}_a \tilde{\Pi}^a (\partial_\mu \partial_\mu \tilde{\Pi}_b) \partial_\nu \partial_\nu \tilde{\Pi}^b \right\}, \quad (30) \end{aligned}$$

where we defined the squared mass of the $\tilde{\Pi}^a$ fields,

$$\mathcal{M}_{\Pi,k}^2 = \frac{\tilde{h}_{\text{ESB}}}{f_\pi}, \quad (31)$$

as well as the low-energy couplings

$$\begin{aligned} \tilde{C}_{1,k} &= \frac{\mathcal{M}_{\Pi,k}^2}{8f_\pi^2}, \\ \tilde{Z}_{2,k} &= -\frac{1}{4f_\pi^2}, \\ \tilde{C}_{3,k} &= \tilde{C}_{3,k} - \tilde{C}_{5,k} + \tilde{C}_{7,k} + 2(\tilde{C}_{6,k} + \tilde{C}_{8,k}), \\ \tilde{C}_{4,k} &= \tilde{C}_{4,k}, \\ \tilde{C}_{5,k} &= 2(\tilde{C}_{6,k} + \tilde{C}_{8,k}), \\ \tilde{C}_{6,k} &= -\tilde{C}_{6,k} - \tilde{C}_{8,k}, \\ \tilde{C}_{8,k} &= \frac{1}{2}(\tilde{C}_{6,k} + \tilde{C}_{8,k}). \end{aligned} \quad (32)$$

It should be underlined that Eq. (30) is calculated from Eq. (26) by integrating several terms by parts in order to reobtain the term structures of the derivative expansion (14).

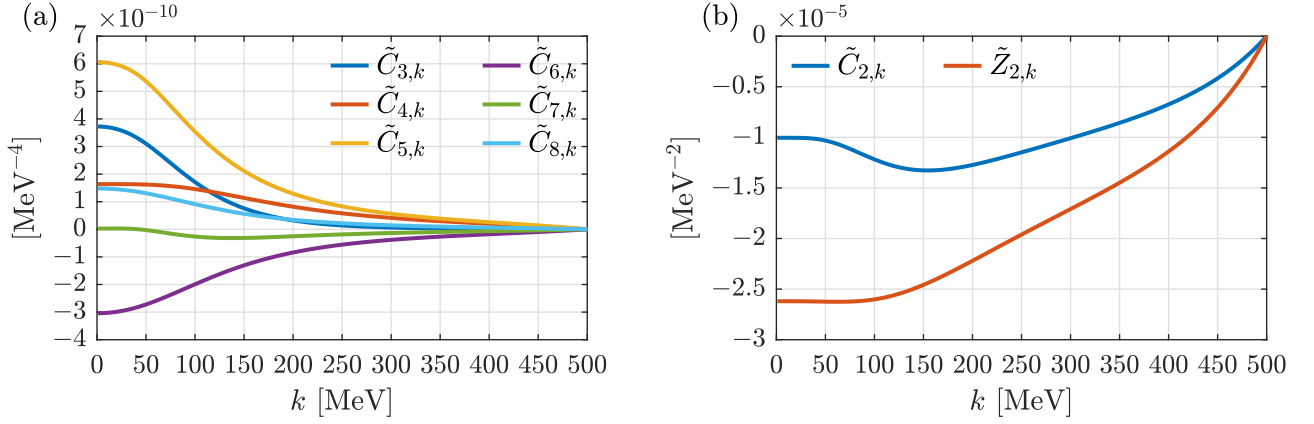


Figure 1. Higher-derivative couplings of the linear QMM. (a) Scale evolution of the renormalized couplings $\tilde{C}_{i,k}$, $i = 3, \dots, 8$. (b) Scale evolution of the renormalized couplings $\tilde{C}_{2,k}$ and $\tilde{Z}_{2,k}$; $k_{\text{IR}} = 1$ MeV.

Equation (30) is one of the central results of this paper. It is the nonlinear counterpart of the linear QMM and, as repeatedly pointed out, has to be understood as its low-energy limit. Moreover, we obtained relations between the low-energy couplings in the linear and the nonlinear model, cf. Eq. (32).

It is remarkable that the geometrical constraint of fixing the $\tilde{\theta}$ field to the constant radius of the three-sphere restricts the number of possible couplings of order $\mathcal{O}(\partial^2)$ as well as $\mathcal{O}(\partial^4)$. In the chosen set of coordinates, only the analogue of $\tilde{Z}_{2,k}$, the coupling $\tilde{Z}_{2,k}$ out of the terms of order $\mathcal{O}(\partial^2)$, “survives” in the nonlinear framework, while the interaction $\sim \tilde{C}_{2,k}$ vanishes. The same holds true for the couplings $\tilde{C}_{3,k}$, $\tilde{C}_{4,k}$, $\tilde{C}_{5,k}$, $\tilde{C}_{6,k}$, and $\tilde{C}_{8,k}$ in the case of the terms of order $\mathcal{O}(\partial^4)$. Besides, it obviously arises a linear dependence in the nonlinear model between the couplings $\tilde{C}_{5,k}$, $\tilde{C}_{6,k}$, and $\tilde{C}_{8,k}$ after fixing the $\tilde{\theta}$ field, see once more Eq. (32).

We observe that the momentum-independent quartic coupling $\tilde{C}_{1,k}$ and the effective potential U_k , in general, do not enter the low-energy limit. Also, the couplings $\tilde{C}_{2,k}$ and $\tilde{Z}_{2,k}$ are irrelevant for the results in the nonlinear effective pion action. They only indirectly influence the result through the integration process of the system of flow equations. Furthermore, the couplings $\tilde{C}_{1,k}$ and $\tilde{Z}_{2,k}$ are identical to the analytical results for the respective terms in the ChPT Lagrangian formulated in stereographic coordinates, as can be easily deduced from Ref. [6]. In fact, within the geometrical constraints on the vacuum manifold, the coupling $\tilde{Z}_{2,k}$ is only a function of the pion decay constant f_π .

IV. NUMERICAL RESULTS AND DISCUSSION

We now present the numerical results for the higher-derivative interactions as obtained from the linear QMM, renormalized at a hadronic cutoff scale of $\Lambda = 500$ MeV, as well as the derived low-energy couplings of the nonlin-

ear model. All additional constituents of truncation (14) and details on their calculation within the FRG framework are described in Appendix C.

A. Linear model: Higher-derivative couplings

The results for the higher-derivative pion couplings of the linear QMM are shown in Fig. 1. The subfigures 1(a) and 1(b) explicitly show how these couplings, initialized at zero in the UV, become nonzero as soon as the RG scale k decreases. Their final numerical values in the IR limit, $k_{\text{IR}} = 1$ MeV, are collected in the column “Linear model” of Table I.

Since the $\mathcal{O}(\partial^2)$ couplings of the nonlinear model do not depend on the corresponding couplings of the linear QMM, we discuss the $\mathcal{O}(\partial^4)$ couplings first. Figure 1(a) reveals that the main contribution to the couplings $\tilde{C}_{i,k}$, $i = 3, \dots, 8$, comes from fluctuations with energy-momentum scales of $k \simeq 50 - 200$ MeV, which is significantly below the scale of spontaneous chiral symmetry breaking; $k_{\text{SSB}} \simeq 300$ MeV. We thus conclude that these couplings are well captured by the low-energy dynam-

Table I. Low-energy (derivative) couplings.^a

Linear model		Nonlinear model	
$\tilde{C}_2 [1/f_\pi^2] \times 10$	-0.88	$\tilde{Z}_2 [1/f_\pi^2] \times 10$...
$\tilde{Z}_2 [1/f_\pi^2] \times 10$	-2.30	$\tilde{C}_3 [1/f_\pi^4] \times 10^2$	-2.50
$\tilde{C}_3 [1/f_\pi^4] \times 10^2$	2.88	$\tilde{C}_4 [1/f_\pi^4] \times 10^2$	-4.20
$\tilde{C}_4 [1/f_\pi^4] \times 10^2$	1.27	$\tilde{C}_5 [1/f_\pi^4] \times 10^2$	1.27
$\tilde{C}_5 [1/f_\pi^4] \times 10^2$	4.69	$\tilde{C}_6 [1/f_\pi^4] \times 10^2$	-2.41
$\tilde{C}_6 [1/f_\pi^4] \times 10^2$	-2.35	$\tilde{C}_7 [1/f_\pi^4] \times 10^2$	1.21
$\tilde{C}_7 [1/f_\pi^4] \times 10^2$	0.02	$\tilde{C}_8 [1/f_\pi^4] \times 10^2$...
$\tilde{C}_8 [1/f_\pi^4] \times 10^2$	1.14	$\tilde{C}_8 [1/f_\pi^4] \times 10^2$	-0.60

^a Values are given at $k = 1$ MeV.

ics of the QMM. Also, given their slow running above the scale of chiral symmetry breaking, the initial value of zero seems to be a very reasonable approximation for these couplings.

Although of less relevance for the low-energy couplings of the nonlinear model, it is still interesting to investigate also the $\mathcal{O}(\partial^2)$ couplings of the linear QMM. As already observed in the preceding investigation [4], these couplings experience a rapid initial change at RG scales close to the UV cutoff. This rapid initial change of the couplings of order $\mathcal{O}(\partial^2)$ is an indication that a hadronic cutoff scale of around 500 MeV is actually too low for a precise determination of these couplings. However, the fixed point-like scale evolution of $\tilde{C}_{2,k}$ and $\tilde{Z}_{2,k}$ at intermediate RG scales suggests that their IR values do not drastically depend on the choice of Λ . In future investigations, the dynamical-hadronization approach [20, 28–30] will allow for a smooth transition between the fundamental interactions and the bosonic operators presented in this study and, in turn, for a computation of these couplings directly from quark and gluon fluctuations at QCD scales, cf. also Refs. [11–13].

B. Nonlinear model: Low-energy couplings

As already argued, the computation of the low-energy limit of the QMM requires the integration of all nonpionic fields. Nevertheless, we present the nontrivial $\mathcal{O}(\partial^4)$ low-energy couplings on all RG scales.

Figure 2 shows the results of applying (32) at every RG scale. Additionally, we have decomposed the contributions to these couplings into quark and meson loops, respectively. Despite the fact that the main contribution to the linear $\mathcal{O}(\partial^4)$ couplings, cf. Fig. 1(a), stems from fluctuations below the scale of chiral symmetry breaking, these couplings are almost exclusively determined by the quark fluctuations. The mesonic fluctuations and, in particular, the pionic fluctuations contribute noticeably to the total couplings only at energies below 200 MeV. However, also in this energy regime, the main contribution is due to quark fluctuations. This is in accordance with functional QCD calculations [11–13] of other low-energy couplings in the linear realization.

The most astonishing observation in Figs. 2(a), 2(b), and 2(c) is that the loop contributions from the quark degrees of freedom are only fully integrated out at scales below 50 – 100 MeV. This is almost certainly also the case in full QCD, since functional QCD calculations [11–13] exhibit an even stronger dominance of qualitatively similar quark fluctuations. Therefore, we conclude that the low-energy couplings can only be determined and defined from QCD below these scales, at least in the used renormalization scheme. Furthermore, this also leads to a natural cutoff scale for theories that are exclusively based on pion fluctuations.

Lastly, a comparison with the according values from ChPT would require compatible renormalization schemes

and comparable renormalization scales. It is also clear that the computed low-energy couplings presented in this work do not yet include the effect of resonances, especially, the light scalar and vector channels.

The numerical IR values of the higher-derivative couplings in the nonlinearly realized effective pion action are listed in the last column (“Nonlinear model”) of Table I. The couplings that vanish in the nonlinear picture are denoted by three dots. The pion mass amounts to $\mathcal{M}_{\pi,k_{\text{IR}}} = 138.5$ MeV. The momentum-independent coupling $\tilde{\mathcal{C}}_{1,k_{\text{IR}}}$ has a value of 0.27.

V. SUMMARY AND OUTLOOK

In this work, we studied the low-energy limit of the $O(4)$ QMM within the FRG approach by transforming the corresponding effective action into an effective pion theory. This corresponds to a transition from the QMM based on a linear realization of the $O(4)$ symmetry to a model where the pions enter according to a nonlinear realization.

Our approach yields precise statements about the energy-momentum scale below which the dynamics is dominated by pionic degrees of freedom. We find that for physical pion masses:

- (i) The pion loop contributions to the low-energy couplings are strongly suppressed as compared to the quark loops.
- (ii) In our renormalization scheme, the scale for the decoupling of the quark fluctuations and, in turn, the range of validity of the low-energy effective theory is roughly given by 50 – 100 MeV.

Due to the qualitative similarity of the QMM dynamics to the low-energy limit of QCD, these statements most likely extrapolate to full QCD, which has to be checked explicitly in a future investigation.

Upcoming studies will also shed more light on the relation to ChPT, where this work can be understood as an extension of Refs. [5, 6]. In particular, it would be very interesting if the computed low-energy couplings of the QMM and related effective theories, like the extended LSM [31], are consistent with the low-energy limit of QCD (the latter is formalized by means of the LECs in ChPT). However, as stated above, this would require a meaningful choice of the renormalization scale in ChPT with regard to the physical relevance of pion fluctuations. Moreover, such a comparison implies a profound discussion of the effect of resonances on the low-energy couplings within our approach. One also has to carefully evaluate how much this comparison would be distorted by the fact that our analysis is formulated in terms of the effective action, which has been generated from the flow of the linearly realized QMM.

Finally, and on a more technical level, the presented work is an extension of our previous exploratory study [4]

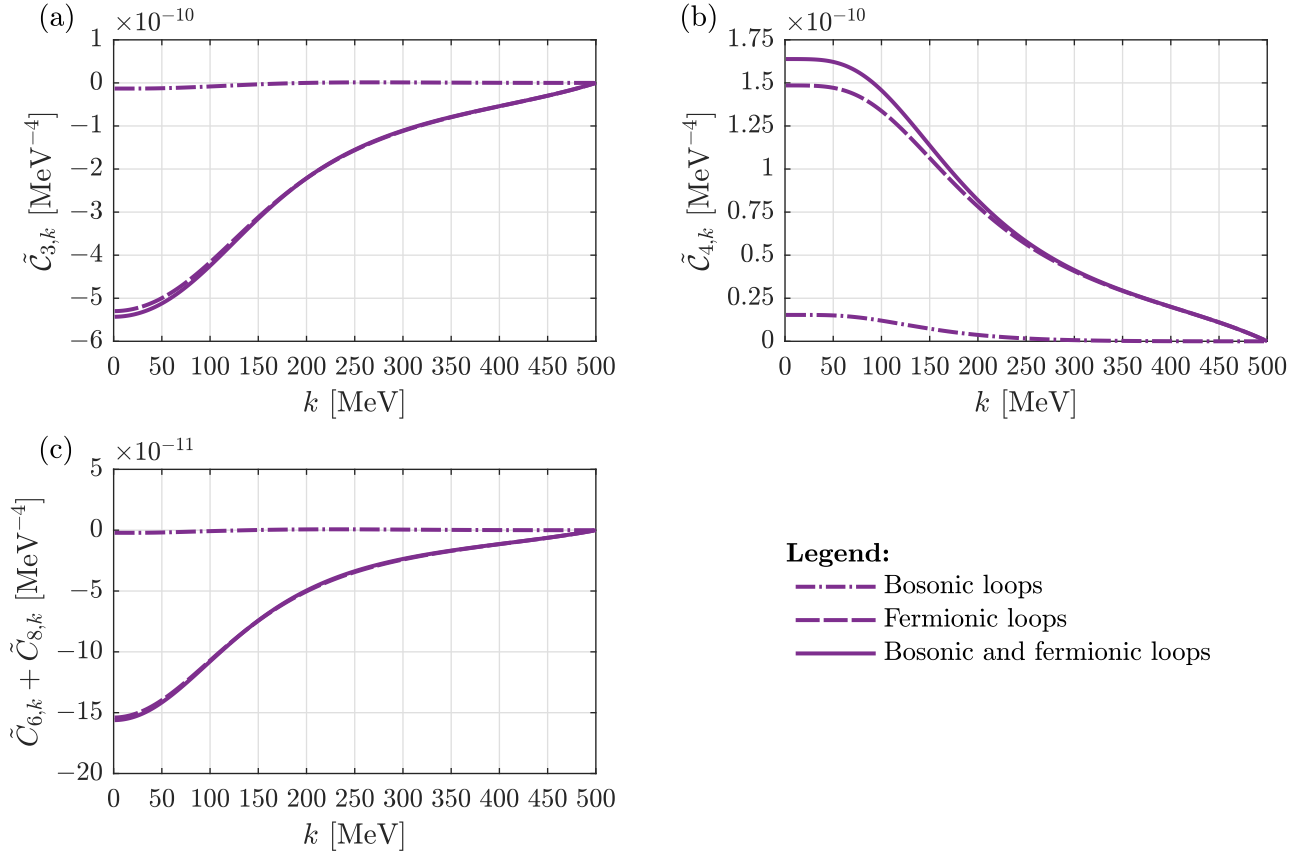


Figure 2. Low-energy couplings of the nonlinear model. (a) and (b) Scale evolution of the renormalized couplings $\tilde{C}_{3,k}$ and $\tilde{C}_{4,k}$, respectively. (c) Scale evolution of $\tilde{C}_{6,k} + \tilde{C}_{8,k}$ representing the renormalized couplings $\tilde{C}_{5,k}$, $\tilde{C}_{6,k}$, and $\tilde{C}_{8,k}$. The evolution of the couplings (solid lines) is decomposed into fermionic (dashed lines) and bosonic contributions (dash-dotted lines); $k_{\text{IR}} = 1$ MeV.

of higher-derivative pion self-interactions within the FRG formalism. The used truncation was improved by including higher-derivative $\sigma\pi$ as well as σ self-interactions in a completely $O(4)$ -symmetric way. Additionally, we took also the flow of the Yukawa coupling into account. All higher-derivative couplings were dynamically generated from the FRG flow, which was initialized at a hadronic scale of 500 MeV. The large corrections of the interactions of order $\mathcal{O}(\partial^2)$ right after the initialization suggests a determination of these couplings from QCD scales in future investigations. Such an analysis could be carried out using the dynamical-hadronization procedure [11–13], which consistently describes mesonic degrees of freedom as quark-antiquark bound states.

ACKNOWLEDGMENTS

The authors thank M. Birse, J.-P. Blaizot, D. D. Dietrich, J. Goity, A. Koenigstein, J. M. Pawłowski, R. D. Pisarski, J. Qiu, S. Rechenberger, F. Rennecke, D. H. Rischke, B.-J. Schaefer, L. von Smekal, and C. Weiss for valuable discussions. J. E. acknowledges funding by the German National Academic Foundation and HIC for

FAIR. M. M. is supported by the DFG grant MI 2240/1-1 and the U.S. Department of Energy under contract de-sc0012704.

Appendix A: Transformation properties

This section is intended to briefly review the transformation properties of the coset representative and the coefficients of the Maurer-Cartan form. It should be noted that $\Sigma(\zeta)$ is an element of $SO(4)$. Acting on the representative from the left by an arbitrary group element $g \in SO(4)$ clearly yields another group element $g\Sigma(\zeta)$. However, the latter object does not belong to the same left coset as $\Sigma(\zeta)$. Generally, the representative of this new coset takes the form $\Sigma(\zeta')h(\zeta, g)$, such that

$$g\Sigma(\zeta) = \Sigma(\zeta')h(\zeta, g), \quad (\text{A1})$$

where $h(\zeta, g) \in SO(3)$ usually depends on the group element $g \in SO(4)$ and the pNGB fields. This implies that $h(\zeta, g)$ depends on spacetime and is therefore a local transformation. Then, Eq. (A1) automatically deter-

mines the transformation behavior of the pNGB fields,

$$\zeta^a \xrightarrow{SO(4)} (\zeta^a)' \equiv f^a(\zeta, g), \quad a = 1, 2, 3, \quad (\text{A2})$$

where the functions f^a depend on the choice of coordinates and, in general, turn out to be nonlinear.

Using Eq. (A1) as well as Eqs. (7) and (8), the transformation properties of the coefficients of the horizontal and vertical part of the Maurer-Cartan form can be derived as

$$e_\mu^a(\zeta) x_a \xrightarrow{SO(4)} h(\zeta, g) e_\mu^a(\zeta) x_a h^{-1}(\zeta, g), \quad (\text{A3})$$

$$\begin{aligned} \omega_\mu^i(\zeta) s_i &\xrightarrow{SO(4)} h(\zeta, g) \omega_\mu^i(\zeta) s_i h^{-1}(\zeta, g) \\ &\quad - i h(\zeta, g) \partial_\mu h^{-1}(\zeta, g). \end{aligned} \quad (\text{A4})$$

In order to illustrate the above formulas by means of an example, we consider the transformation properties of the field variables of the models discussed in Secs. II A and III B. To this end, we start with the Lie algebra $\mathfrak{so}(4)$ and choose its basis according to

$$\begin{aligned} [s_i, s_j] &= i \epsilon_{ij}^{k} s_k, \\ [s_i, x_b] &= i \epsilon_{ib}^{c} x_c, \\ [x_a, x_b] &= i \epsilon_{ab}^{k} s_k, \end{aligned} \quad (\text{A5})$$

where the indices $i, j, k = 1, 2, 3$ label the generators s_i of the unbroken $SO(3)$ subgroup and where $a, b, c = 1, 2, 3$ label the coset generators x_a . An explicit realization of this basis is given by

$$\begin{aligned} s_1 &= \begin{pmatrix} 0 & 0 & 0 & 0 \\ 0 & 0 & -i & 0 \\ 0 & i & 0 & 0 \\ 0 & 0 & 0 & 0 \end{pmatrix}, & x_1 &= \begin{pmatrix} 0 & 0 & 0 & -i \\ 0 & 0 & 0 & 0 \\ 0 & 0 & 0 & 0 \\ i & 0 & 0 & 0 \end{pmatrix}, \\ s_2 &= \begin{pmatrix} 0 & 0 & i & 0 \\ 0 & 0 & 0 & 0 \\ -i & 0 & 0 & 0 \\ 0 & 0 & 0 & 0 \end{pmatrix}, & x_2 &= \begin{pmatrix} 0 & 0 & 0 & 0 \\ 0 & 0 & 0 & -i \\ 0 & 0 & 0 & 0 \\ 0 & i & 0 & 0 \end{pmatrix}, \\ s_3 &= \begin{pmatrix} 0 & -i & 0 & 0 \\ i & 0 & 0 & 0 \\ 0 & 0 & 0 & 0 \\ 0 & 0 & 0 & 0 \end{pmatrix}, & x_3 &= \begin{pmatrix} 0 & 0 & 0 & 0 \\ 0 & 0 & 0 & 0 \\ 0 & 0 & 0 & -i \\ 0 & 0 & i & 0 \end{pmatrix}. \end{aligned} \quad (\text{A6})$$

The normalization of the above generators is chosen such that

$$\begin{aligned} \text{tr}(s_i s_j) &= 2\delta_{ij}, \\ \text{tr}(x_a x_b) &= 2\delta_{ab}, \\ \text{tr}(s_i x_a) &= 0, \end{aligned} \quad (\text{A7})$$

for all $i, j = 1, 2, 3$ and $a, b = 1, 2, 3$.

Now, we consider an infinitesimal $SO(4)$ transformation

$$O \simeq \mathbb{1}_4 - i\alpha^i s_i - i\beta^a x_a, \quad (\text{A8})$$

where α^i and β^a denote the group parameters. Using the isomorphism $SO(4) \cong SU(2) \times SU(2)$ as well as Eq. (2), one obtains

$$\pi^a \xrightarrow{SU(2)_V} \pi^a + \epsilon_{jc}^{a} \alpha^j \pi^c, \quad \sigma \xrightarrow{SU(2)_V} \sigma, \quad (\text{A9})$$

$$\pi^a \xrightarrow{SU(2)_A} \pi^a - \beta^a \sigma, \quad \sigma \xrightarrow{SU(2)_A} \sigma + \beta_a \pi^a, \quad (\text{A10})$$

which is the usual transformation behavior of the σ field and the pions. From these results and by using Eq. (21), it is possible to derive the transformation behavior of the nonlinear fields. For the radial field θ , one obtains

$$\theta \xrightarrow{SU(2)_V} \theta, \quad \theta \xrightarrow{SU(2)_A} \theta, \quad (\text{A11})$$

while the pNGB fields transform as

$$\zeta^a \xrightarrow{SU(2)_V} \zeta^a + \epsilon_{jc}^{a} \alpha^j \zeta^c, \quad (\text{A12})$$

$$\zeta^a \xrightarrow{SU(2)_A} \zeta^a - \frac{\beta^a}{2} (1 - \zeta_b \zeta^b) - \zeta^a (\beta_b \zeta^b), \quad (\text{A13})$$

cf. Eq. (A2). It is a general result that the pNGB fields transform in a linear representation with respect to the unbroken subgroup, whereas for coset transformations their transformation behavior becomes nonlinear.

Appendix B: Flow equations

The regulators R_k in the Wetterich equation (12) effectively separate the low-energy modes in momentum space from the integration process by introducing an additional mass term. As a function of the RG scale k and the momentum q , they fulfill the limits

$$R_k \rightarrow 0 \text{ for } k \rightarrow 0, \quad (\text{B1})$$

$$R_k \rightarrow \infty \text{ for } k \rightarrow \Lambda \rightarrow \infty, \quad (\text{B2})$$

$$R_k > 0 \text{ for } q \rightarrow 0, \quad (\text{B3})$$

$$R_k \rightarrow 0 \text{ for } q \rightarrow \infty. \quad (\text{B4})$$

The explicit expressions for the bosonic and fermionic regulators used in this work read

$$R_k^\sigma(q^2) = Z_k^\sigma q^2 r\left(\frac{q^2}{k^2}\right), \quad (\text{B5})$$

$$R_k^\pi(q^2) = Z_k^\pi q^2 r\left(\frac{q^2}{k^2}\right), \quad (\text{B6})$$

$$R_k^\psi(q) = -i Z_k^\psi \gamma_\mu q_\mu r\left(\frac{q^2}{k^2}\right), \quad (\text{B7})$$

where we employ an exponential shape function r of the generic form [14, 32–35]

$$r(x) = \frac{x^{m-1}}{\exp(x^m) - 1}, \quad (\text{B8})$$

with $m = 1$ for both bosonic and fermionic degrees of freedom.

The flow equations for the (unrenormalized) scale-dependent quantities corresponding to truncation (14) are derived from the Wetterich equation (12) as follows [partly using a diagrammatic representation analogously to Eq. (13); \mathcal{V} denotes the infinite spacetime volume]:

$$\partial_k U_k = \mathcal{V}^{-1} \partial_k \Gamma_k = \mathcal{V}^{-1} \left(\frac{1}{2} \text{diagram}_\sigma + \frac{1}{2} \text{diagram}_\pi - \text{diagram}_\psi \right), \quad (\text{B9})$$

$$\begin{aligned} \partial_k y_k &= \frac{1}{2} \mathcal{V}^{-1} \frac{1}{\sigma} \text{tr}_\gamma \left[\frac{\delta}{\delta \bar{\psi}(0)} \partial_k \Gamma_k \frac{\overleftarrow{\delta}}{\delta \psi(0)} \right] \\ &= \frac{1}{2} \mathcal{V}^{-1} \frac{1}{\sigma} \text{tr}_\gamma \left(\frac{1}{2} \text{diagram}_{\sigma\psi} + \frac{1}{2} \text{diagram}_{\pi\psi} - \text{diagram}_{\psi\sigma} - \text{diagram}_{\psi\pi} \right), \end{aligned} \quad (\text{B10})$$

$$\begin{aligned} \partial_k Z_k^\sigma &= \mathcal{V}^{-1} \frac{d}{dp^2} \Big|_{p^2=0} \frac{\delta^2 \partial_k \Gamma_k}{\delta \sigma(-p) \delta \sigma(p)} \\ &= \mathcal{V}^{-1} \frac{d}{dp^2} \Big|_{p^2=0} \left(\frac{1}{2} \text{diagram}_{\sigma\sigma} + \frac{1}{2} \text{diagram}_{\pi\pi} - \text{diagram}_{\psi\psi} \right. \\ &\quad \left. - \frac{1}{2} \text{diagram}_{\sigma\sigma} - \frac{1}{2} \text{diagram}_{\pi\pi} \right), \end{aligned} \quad (\text{B11})$$

$$\begin{aligned} \partial_k Z_k^\pi &= \mathcal{V}^{-1} \frac{d}{dp^2} \Big|_{p^2=0} \frac{\delta^2 \partial_k \Gamma_k}{\delta \pi_1(-p) \delta \pi_1(p)} \\ &= \mathcal{V}^{-1} \frac{d}{dp^2} \Big|_{p^2=0} \left(\frac{1}{2} \text{diagram}_{\pi\pi} + \frac{1}{2} \text{diagram}_{\sigma\sigma} - \text{diagram}_{\psi\psi} \right. \\ &\quad \left. - \frac{1}{2} \text{diagram}_{\sigma\sigma} - \frac{1}{2} \text{diagram}_{\pi\pi} \right), \end{aligned} \quad (\text{B12})$$

$$\begin{aligned} \partial_k Z_k^\psi &= \frac{i}{4} \mathcal{V}^{-1} \frac{d}{dp^2} \Big|_{p^2=0} \text{tr}_\gamma \left[\frac{\delta}{\delta \bar{\psi}(p)} \partial_k \Gamma_k \frac{\overleftarrow{\delta}}{\delta \psi(p)} \gamma_\mu p_\mu \right] \\ &= \frac{i}{4} \mathcal{V}^{-1} \frac{d}{dp^2} \Big|_{p^2=0} \text{tr}_\gamma \left[\left(\frac{1}{2} \text{diagram}_{\sigma\psi} + \frac{1}{2} \text{diagram}_{\pi\psi} \right) \right] \end{aligned}$$

$$- \left(\begin{array}{c} \text{Diagram 1: } \psi \text{ lines, } \sigma \text{ loop} \\ \text{Diagram 2: } \psi \text{ lines, } \pi \text{ loop} \end{array} \right) \gamma_\mu p_\mu \Bigg], \quad (\text{B13})$$

$$\begin{aligned} \partial_k C_{2,k} &= \frac{1}{2} \mathcal{V}^{-1} \frac{d}{dp^2} \Big|_{p^2=0} \frac{\delta^4 \partial_k \Gamma_k}{\delta \pi_1(p) \delta \pi_2(-p) \delta \pi_1(0) \delta \pi_2(0)} \\ &= \frac{1}{2} \mathcal{V}^{-1} \frac{d}{dp^2} \Big|_{p^2=0} \left(\begin{array}{l} -\frac{1}{2} \text{Diagram 1} - \frac{1}{2} \text{Diagram 2} \\ +\frac{1}{2} \text{Diagram 3} + \frac{1}{2} \text{Diagram 4} - \frac{1}{2} \text{Diagram 5} \\ -\frac{1}{2} \text{Diagram 6} - \frac{1}{2} \text{Diagram 7} - \frac{1}{2} \text{Diagram 8} \\ +\frac{1}{2} \text{Diagram 9} + \frac{1}{2} \text{Diagram 10} - \text{Diagram 11} \end{array} \right), \quad (\text{B14}) \end{aligned}$$

$$\partial_k Z_{2,k} = \frac{1}{4} \mathcal{V}^{-1} \frac{d}{dp^2} \Big|_{p^2=0} \frac{\delta^4 \partial_k \Gamma_k}{\delta \pi_1(p) \delta \pi_2(0) \delta \pi_1(-p) \delta \pi_2(0)}, \quad (\text{B15})$$

$$\partial_k C_{3,k} = \frac{5}{576} \left\{ \frac{208}{5} \partial_k C_{5,k} - 112 \partial_k C_{6,k} + 32 \partial_k C_{7,k} - \frac{224}{5} \partial_k C_{8,k} + \mathcal{V}^{-1} \left(\frac{\partial}{\partial p_{1,\mu}} \frac{\partial}{\partial p_{2,\mu}} \frac{\partial}{\partial p_{3,\nu}} \frac{\partial}{\partial p_{1,\nu}} \right. \right. \\ \left. \left. - \frac{7}{10} \frac{\partial}{\partial p_{1,\mu}} \frac{\partial}{\partial p_{2,\mu}} \frac{\partial}{\partial p_{3,\nu}} \frac{\partial}{\partial p_{2,\nu}} \right) \Big|_{p_1=p_2=p_3=0} \frac{\delta^4 \partial_k \Gamma_k}{\delta \pi_1(p_1) \delta \pi_2(p_2) \delta \pi_1(p_3) \delta \pi_2(-p_1-p_2-p_3)} \right\}, \quad (\text{B16})$$

$$\partial_k C_{4,k} = -\frac{1}{288} \left\{ -16 \partial_k C_{5,k} - 400 \partial_k C_{6,k} + 32 \partial_k C_{7,k} - 160 \partial_k C_{8,k} + \mathcal{V}^{-1} \left(\frac{\partial}{\partial p_{1,\mu}} \frac{\partial}{\partial p_{2,\mu}} \frac{\partial}{\partial p_{3,\nu}} \frac{\partial}{\partial p_{1,\nu}} \right. \right. \\ \left. \left. - \frac{5}{2} \frac{\partial}{\partial p_{1,\mu}} \frac{\partial}{\partial p_{2,\mu}} \frac{\partial}{\partial p_{3,\nu}} \frac{\partial}{\partial p_{2,\nu}} \right) \Big|_{p_1=p_2=p_3=0} \frac{\delta^4 \partial_k \Gamma_k}{\delta \pi_1(p_1) \delta \pi_2(p_2) \delta \pi_1(p_3) \delta \pi_2(-p_1-p_2-p_3)} \right\}, \quad (\text{B17})$$

$$\partial_k C_{5,k} = \frac{1}{96} \mathcal{V}^{-1} \left(\frac{\partial}{\partial p_{2,\mu}} \frac{\partial}{\partial p_{2,\mu}} \frac{\partial}{\partial p_{2,\nu}} \frac{\partial}{\partial p_{3,\nu}} \right. \\ \left. - \frac{1}{2} \frac{\partial}{\partial p_{2,\mu}} \frac{\partial}{\partial p_{2,\mu}} \frac{\partial}{\partial p_{2,\nu}} \frac{\partial}{\partial p_{2,\nu}} \right) \Big|_{p_2=p_3=0} \frac{\delta^4 \partial_k \Gamma_k}{\delta \pi_1(-p_2-p_3) \delta \pi_2(p_2) \delta \pi_1(p_3) \delta \pi_2(0)}, \quad (\text{B18})$$

$$\partial_k C_{6,k} = -\frac{1}{96} \left\{ 160 \partial_k C_{5,k} + 64 \partial_k C_{7,k} + \mathcal{V}^{-1} \frac{\partial}{\partial p_{2,\mu}} \frac{\partial}{\partial p_{4,\mu}} \frac{\partial}{\partial p_{2,\nu}} \frac{\partial}{\partial p_{4,\nu}} \Big|_{p_2=p_4=0} \frac{\delta^4 \partial_k \Gamma_k}{\delta \pi_1(-p_2-p_4) \delta \pi_2(p_2) \delta \pi_1(0) \delta \pi_2(p_4)} \right. \\ \left. - \frac{1}{12} \mathcal{V}^{-1} \frac{\partial}{\partial p_\mu} \frac{\partial}{\partial p_\mu} \frac{\partial}{\partial p_\nu} \frac{\partial}{\partial p_\nu} \Big|_{p=0} \frac{\delta^4 \partial_k \Gamma_k}{\delta \pi_1(-p) \delta \pi_2(0) \delta \pi_1(p) \delta \pi_2(0)} \right\}, \quad (\text{B19})$$

$$\partial_k C_{7,k} = -\frac{1}{384} \mathcal{V}^{-1} \frac{\partial}{\partial p_\mu} \frac{\partial}{\partial p_\mu} \frac{\partial}{\partial p_\nu} \frac{\partial}{\partial p_\nu} \Big|_{p=0} \frac{\delta^4 \partial_k \Gamma_k}{\delta \pi_1(-p) \delta \pi_2(p) \delta \pi_1(0) \delta \pi_2(0)}, \quad (\text{B20})$$

$$\partial_k C_{8,k} = \frac{1}{96} \left\{ 160 \partial_k C_{5,k} + 64 \partial_k C_{7,k} + \mathcal{V}^{-1} \frac{\partial}{\partial p_{2,\mu}} \frac{\partial}{\partial p_{4,\mu}} \frac{\partial}{\partial p_{2,\nu}} \frac{\partial}{\partial p_{4,\nu}} \Big|_{p_2=p_4=0} \frac{\delta^4 \partial_k \Gamma_k}{\delta \pi_1(-p_2-p_4) \delta \pi_2(p_2) \delta \pi_1(0) \delta \pi_2(p_4)} \right. \\ \left. - \frac{5}{24} \mathcal{V}^{-1} \frac{\partial}{\partial p_\mu} \frac{\partial}{\partial p_\mu} \frac{\partial}{\partial p_\nu} \frac{\partial}{\partial p_\nu} \Big|_{p=0} \frac{\delta^4 \partial_k \Gamma_k}{\delta \pi_1(-p) \delta \pi_2(0) \delta \pi_1(p) \delta \pi_2(0)} \right\}. \quad (\text{B21})$$

As before, p or p_i with $i \in \{1, 2, 3, 4\}$ represents the external momentum of the corresponding leg. The diagrams shown on the right side of the equations include all possible permutations of the external fields. Five- and six-point vertices are truncated.

Note that the wave-function renormalizations Z_k^σ and Z_k^π defined in Eqs. (16) and (17) are evaluated at vanishing external momentum, $p^2 = 0$, i.e.,

$$Z_k^\sigma = Z_k + 2\sigma^2 (Z_{2,k} + C_{2,k}), \quad (\text{B22})$$

$$Z_k^\pi = Z_k + 2\sigma^2 Z_{2,k}. \quad (\text{B23})$$

Due to the full $O(4)$ -symmetric truncation in Eq. (14), the equations of Z_k^σ and Z_k^π also include all diagrams with momentum-dependent four-point vertices. This is in contrast to Ref. [4], where we only considered momentum-dependent four-pion interactions.

To derive the analytical flow equations we made use of the **Mathematica** packages **FeynCalc** [36, 37], **DoFun** [38], and **FormTracer** [39].

Appendix C: Solving the flow equations

We solve the system of coupled flow equations using a Taylor-polynomial ansatz for the effective potential,

$$U_k(\rho) = \sum_{n=1}^N \frac{\alpha_{n,k}}{n!} (\rho - \chi)^n, \quad (\text{C1})$$

where the expansion point χ is scale independent. This choice of χ follows the considerations of Ref. [40]. The ansatz (C1) leads to stable results for $N = 6$, in the sense that the Taylor solution coincides with the results from a grid discretization.

The flow equations for the Taylor coefficients $\alpha_{n,k}$ are obtained from derivatives of the flow equation of the effective potential,

$$\partial_k \alpha_{n,k} = \frac{\partial^n}{\partial \rho^n} \Big|_{\chi} \partial_k U_k. \quad (\text{C2})$$

The equations for the wave-function renormalization factors, the Yukawa coupling, and the higher-derivative couplings are also evaluated at the constant expansion point χ , which is chosen to be slightly larger than the IR minimum ρ_0 of the potential.

We initialize the set of flow equations at the UV cutoff $\Lambda = 500$ MeV, which is a typical scale for the QMM and

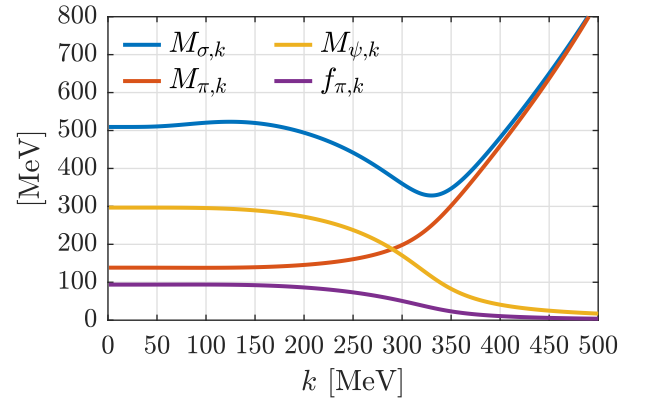


Figure 3. Scale evolution of the renormalized sigma, pion, and quark masses, as well as the pion decay constant; $k_{\text{IR}} = 1$ MeV.

other NJL-like models. In order to capture quark dynamics, this scale somewhat exceeds the ones suggested

Table II. UV parameters ($\Lambda = 500$ MeV).

χ	$\alpha_{1,\Lambda}$	$\alpha_{2,\Lambda}$	h_{ESB}	y_Λ
61.34 ² MeV ²	600 ² MeV ²	1.4	2.75×10^6 MeV ³	8.96

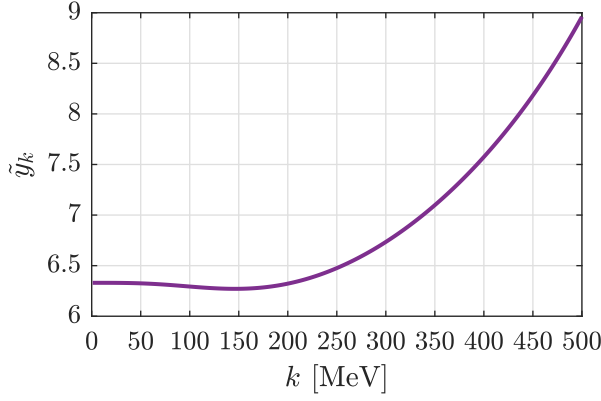


Figure 4. Scale evolution of the renormalized Yukawa coupling \tilde{y}_k ; $k_{\text{IR}} = 1$ MeV.

by recent investigations [11–13], which have shown that the range of validity of these models is around 300 MeV.

At the cutoff Λ , the effective potential is tuned such that we reproduce experimental data for the meson and quark masses as well as for the pion decay constant in the IR, cf. Ref. [41]. The final parameters of this tuning process, including the ESB parameter h_{ESB} and the Yukawa coupling y_Λ , are quoted in Table II. The coefficients $\alpha_{n,\Lambda}$, which are not shown, are set to zero, i.e., $\alpha_{n,\Lambda} = 0$ for $2 < n \leq 6$.

The wave-function renormalization factors are initialized with a value of one and the higher-derivative couplings start at zero in the UV. This means that the couplings $\tilde{C}_{2,k}$ and $\tilde{Z}_{2,k}$, as well as $\tilde{C}_{i,k}$, $i = 3, \dots, 8$, are only dynamically generated during the integration from the UV to the IR.

The scale-dependent “bare” masses of the σ , π , and quark fields are computed from the effective potential. They read

$$m_{\sigma,k}^2 = 2U'_k(\rho_{0,k}) + 4\rho_{0,k}U''_k(\rho_{0,k}), \quad (\text{C3})$$

$$m_{\pi,k}^2 = 2U'_k(\rho_{0,k}), \quad (\text{C4})$$

$$m_{\psi,k}^2 = \frac{y_k^2}{4}\rho_{0,k}, \quad (\text{C5})$$

where $\rho_{0,k}$ denotes the scale-dependent minimum of the potential

$$U_k(\rho) - h_{\text{ESB}}\sqrt{\rho}. \quad (\text{C6})$$

It is related to the pion decay constant via the PCAC relation [4],

$$f_{\pi,k} = \sqrt{Z_k^\pi \rho_{0,k}} \equiv \sqrt{Z_k^\pi} \sigma_{0,k}, \quad (\text{C7})$$

where $\sigma_{0,k}$ denotes the scale-dependent vacuum expectation value of the σ field. The renormalized masses corresponding to Eqs. (C3), (C4), and (C5) are given by

$$M_{\sigma,k}^2 = \frac{m_{\sigma,k}^2}{Z_k^\sigma}, \quad M_{\pi,k}^2 = \frac{m_{\pi,k}^2}{Z_k^\pi}, \quad M_{\psi,k}^2 = \frac{m_{\psi,k}^2}{(Z_k^\psi)^2}. \quad (\text{C8})$$

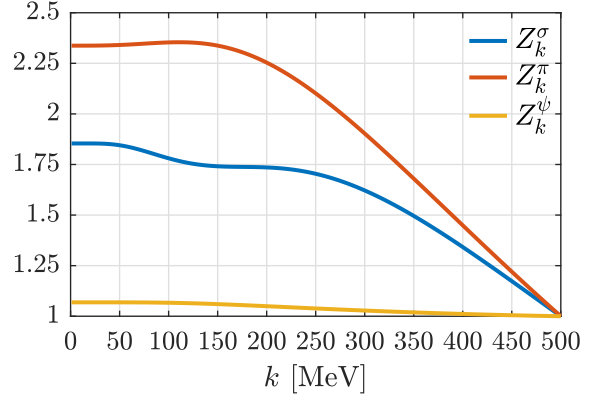


Figure 5. Scale evolution of the bosonic and fermionic wave-function renormalization factors Z_k^σ , Z_k^π , and Z_k^ψ ; $k_{\text{IR}} = 1$ MeV.

After the initialization of the flow, the system of equations is integrated down to 1 MeV, which is a valid IR cutoff less than one percent of Λ , at which all k -dependent quantities are entirely frozen out.

Figure 3 shows the scale dependence of the renormalized masses and the pion decay constant, which is related to the expectation value of the sigma field via Eq. (C7). The latter serves as an (approximate) order parameter for the dynamical $O(4)$ -symmetry breaking [the $O(4)$ invariance of the model is also explicitly broken by the parameter $h_{\text{ESB}} \neq 0$].

In the regime close to the UV, the mesonic fields are approximately degenerate in mass. This is required by the almost restored $O(4)$ symmetry, as indicated by the small value of the expectation value of the sigma field. The quarks are comparatively light in the same regime and they therefore dominate the RG flow.

For lower energies, the QMM undergoes a crossover transition and, hence, the spontaneous breaking of the $O(4)$ symmetry becomes increasingly obvious. At $k \lesssim 50$ MeV, the renormalized masses as well as the pion decay constant approach their “physical” IR-limit values: $M_{\sigma,k_{\text{IR}}} = 509.4$ MeV, $M_{\pi,k_{\text{IR}}} \equiv \mathcal{M}_{\Pi,k_{\text{IR}}} = 138.5$ MeV, $M_{\psi,k_{\text{IR}}} = 296.8$ MeV, and $f_{\pi,k_{\text{IR}}} \equiv f_\pi = 93.8$ MeV.

In Fig. 4 we present the RG flow of the renormalized Yukawa coupling \tilde{y}_k . Starting with a value of 8.96 at the UV scale, it shrinks during the integration and picks up a value of 6.33 in the IR.

The bosonic and fermionic wave-function renormalization factors, Z_k^σ , Z_k^π , and Z_k^ψ , respectively, are plotted in Fig. 5. The numerical values of Z_k^π and Z_k^ψ give the correction from unrenormalized to renormalized quantities in Eq. (18), e.g., the higher-derivative couplings $\tilde{C}_{2,k}$, $\tilde{Z}_{2,k}$, and $\tilde{C}_{i,k}$, $i = 3, \dots, 8$, differ from $C_{2,k}$, $Z_{2,k}$, and $C_{i,k}$, $i = 3, \dots, 8$, by a factor of $1/(Z_k^\pi)^2 \simeq 0.18$ in the IR; $Z_{\pi,k_{\text{IR}}} = 2.34$. In contrast to the bosonic fields, the quark-field renormalization remains moderate, $Z_k^\psi = 1.07$ at $k = 1$ MeV. The factor Z_k^σ , see also Fig. 5, has an IR value of 1.85. The bosonic wave-function renormal-

ization factors are evaluated at the constant expansion point $\chi \equiv \sigma^2$, as introduced in the Taylor polynomial in

Eq. (C1), and, therefore, necessarily differ over the entire k range.

-
- [1] J. Gasser and H. Leutwyler, *Annals Phys.* **158**, 142 (1984).
- [2] J. Gasser and H. Leutwyler, *Nucl. Phys.* **B250**, 465 (1985).
- [3] M. Gell-Mann and M. Levy, *Nuovo Cim.* **16**, 705 (1960).
- [4] J. Eser, F. Divotgey, M. Mitter, and D. H. Rischke, *Phys. Rev.* **D98**, 014024 (2018), arXiv:1804.01787 [hep-ph].
- [5] D. U. Jungnickel and C. Wetterich, *Eur. Phys. J.* **C2**, 557 (1998), arXiv:hep-ph/9704345 [hep-ph].
- [6] F. Divotgey, P. Kovacs, F. Giacosa, and D. H. Rischke, *Eur. Phys. J.* **A54**, 5 (2018), arXiv:1605.05154 [hep-ph].
- [7] K. Meetz, *J. Math. Phys.* **10**, 589 (1969).
- [8] S. Weinberg, *Phys. Rev.* **166**, 1568 (1968).
- [9] S. R. Coleman, J. Wess, and B. Zumino, *Phys. Rev.* **177**, 2239 (1969).
- [10] C. G. Callan, Jr., S. R. Coleman, J. Wess, and B. Zumino, *Phys. Rev.* **177**, 2247 (1969).
- [11] J. Braun, L. Fister, J. M. Pawłowski, and F. Rennecke, *Phys. Rev.* **D94**, 034016 (2016), arXiv:1412.1045 [hep-ph].
- [12] M. Mitter, J. M. Pawłowski, and N. Strodthoff, *Phys. Rev.* **D91**, 054035 (2015), arXiv:1411.7978 [hep-ph].
- [13] A. K. Cyrol, M. Mitter, J. M. Pawłowski, and N. Strodthoff, *Phys. Rev.* **D97**, 054006 (2018), arXiv:1706.06326 [hep-ph].
- [14] C. Wetterich, *Phys. Lett.* **B301**, 90 (1993).
- [15] M. Bonini, M. D’Attanasio, and G. Marchesini, *Nucl. Phys.* **B409**, 441 (1993), arXiv:hep-th/9301114 [hep-th].
- [16] U. Ellwanger, *Proceedings, Workshop on Quantum field theoretical aspects of high energy physics: Bad Frankenhausen, Germany, September 20-24, 1993*, *Z. Phys.* **C62**, 503 (1994), [206(1993)], arXiv:hep-ph/9308260 [hep-ph].
- [17] T. R. Morris, *Int. J. Mod. Phys.* **A9**, 2411 (1994), arXiv:hep-ph/9308265 [hep-ph].
- [18] C. Bagnuls and C. Bervillier, *Phys. Rept.* **348**, 91 (2001), arXiv:hep-th/0002034 [hep-th].
- [19] J. Berges, N. Tetradis, and C. Wetterich, *Phys. Rept.* **363**, 223 (2002), arXiv:hep-ph/0005122 [hep-ph].
- [20] J. M. Pawłowski, *Annals Phys.* **322**, 2831 (2007), arXiv:hep-th/0512261 [hep-th].
- [21] J.-P. Blaizot, A. Ipp, R. Mendez-Galain, and N. Wschebor, *Nucl. Phys.* **A784**, 376 (2007), arXiv:hep-ph/0610004 [hep-ph].
- [22] H. Gies, *Renormalization group and effective field theory approaches to many-body systems*, *Lect. Notes Phys.* **852**, 287 (2012), arXiv:hep-ph/0611146 [hep-ph].
- [23] B.-J. Schaefer and J. Wambach, *Helmholtz International Summer School on Dense Matter in Heavy Ion Collisions and Astrophysics Dubna, Russia, August 21-September 1, 2006*, *Phys. Part. Nucl.* **39**, 1025 (2008), arXiv:hep-ph/0611191 [hep-ph].
- [24] P. Kopietz, L. Bartosch, and F. Schütz, *Lect. Notes Phys.* **798**, 1 (2010).
- [25] L. von Smekal, *Physics at all scales: The Renormalization Group. Proceedings, 49. Internationale Universitätswochen für Theoretische Physik, Winter School: Schladming, Austria, February 26-March 5, 2011*, *Nucl. Phys. Proc. Suppl.* **228**, 179 (2012), arXiv:1205.4205 [hep-ph].
- [26] R. Percacci and O. Zanusso, *Phys. Rev.* **D81**, 065012 (2010), arXiv:0910.0851 [hep-th].
- [27] R. Flore, A. Wipf, and O. Zanusso, *Phys. Rev.* **D87**, 065019 (2013), arXiv:1207.4499 [hep-th].
- [28] H. Gies and C. Wetterich, *Phys. Rev.* **D65**, 065001 (2002), arXiv:hep-th/0107221 [hep-th].
- [29] H. Gies and C. Wetterich, *Phys. Rev.* **D69**, 025001 (2004), arXiv:hep-th/0209183 [hep-th].
- [30] S. Floerchinger and C. Wetterich, *Phys. Lett.* **B680**, 371 (2009), arXiv:0905.0915 [hep-th].
- [31] D. Parganlija, P. Kovacs, G. Wolf, F. Giacosa, and D. H. Rischke, *Phys. Rev.* **D87**, 014011 (2013), arXiv:1208.0585 [hep-ph].
- [32] C. Wetterich, *Nucl. Phys.* **B352**, 529 (1991).
- [33] D. F. Litim, *JHEP* **11**, 059 (2001), arXiv:hep-th/0111159 [hep-th].
- [34] I. Nandori, *JHEP* **04**, 150 (2013), arXiv:1208.5021 [hep-th].
- [35] J. M. Pawłowski, M. M. Scherer, R. Schmidt, and S. J. Wetzel, *Annals Phys.* **384**, 165 (2017), arXiv:1512.03598 [hep-th].
- [36] R. Mertig, M. Böhm, and A. Denner, *Comput. Phys. Commun.* **64**, 345 (1991).
- [37] V. Shtabovenko, R. Mertig, and F. Orellana, *Comput. Phys. Commun.* **207**, 432 (2016), arXiv:1601.01167 [hep-ph].
- [38] M. Q. Huber and J. Braun, *Comput. Phys. Commun.* **183**, 1290 (2012), arXiv:1102.5307 [hep-th].
- [39] A. K. Cyrol, M. Mitter, and N. Strodthoff, *Comput. Phys. Commun.* **219**, 346 (2017), arXiv:1610.09331 [hep-ph].
- [40] J. M. Pawłowski and F. Rennecke, *Phys. Rev.* **D90**, 076002 (2014), arXiv:1403.1179 [hep-ph].
- [41] M. Tanabashi *et al.* (Particle Data Group), *Phys. Rev.* **D98**, 030001 (2018).